19(8-9): 849-854, 2008" which should be cited to refer to this work.

Cobalt substituted ZnO thin films: a potential candidate for spintronics

Kanwal Preet Bhatti · Vivek Kumar Malik · Sujeet Chaudhary

Abstract Cobalt doped zinc oxide thin films have been deposited using spray pyrolysis method. These single phasic films exhibited [100] preferential texture and small decrease in the lattice parameter on cobalt substitution. The films having different Co concentration have almost similar surface morphology and microstructure. These $Zn_{1-x}Co_xO$ ($x \leq 0.10$) thin films distinctly showed ferromagnetic character at room temperature. The optical transmission measurements of these films clearly proved that in these films Co substitutes for Zn^{2+} and exists in +2 state. Based on the optical, structural and magnetic measurements, the possibility of occurrence of ferromagnetic ordering due to cobalt clustering is ruled out in these spray-pyrolyzed films. A correlation of the observed ferromagnetic behavior in these $Zn_{1-x}Co_xO$ films with structural change resulting from the addition of Co is presented in this paper.

1 Introduction

In the past few years, transition metal substituted II–VI oxide semiconductors, namely ZnO, SnO_2 etc., have attracted a renewed research interest due to the prediction of room temperature ferromagnetism (RTFM) in them [1, 2]. The RTFM observed in these oxide semiconductors has opened a new window for potential application of these materials in realization of spintronic devices. However, the experimental findings on the room temperature ferromagnetic ordering in transition metal doped oxide semiconductors reported so far are at large variance and the nature (i.e., extrinsic or intrinsic) and origin of room temperature ferromagnetism is yet far from being clearly understood [3–18]. In our earlier study on chemically synthesized nanocrystalline ZnO:Co powder samples [3–5], we have established the presence of RTFM in these samples as an intrinsic effect. The observed RTFM is certainly not due to cobalt clustering, and has been explained on the basis of the bound magnetic polaron model.

Akin to the case of bulk ZnO:Co samples, the experimental results regarding the presence and origin of RTFM in case of thin films are equally divergent. In case of thin films, though there exist many reports of RTFM in Co doped ZnO films [6–15]. In one case, giant magnetic moment of 6.1 μ_B/Co has been reported in the insulating ZnO:Co thin films [6], whereas in some other cases, RTFM is either claimed to be carrier mediated [7, 8] or attributed to the presence of Co clusters [13–15]. Contrary to the above, ZnO:Co films are reported to be paramagnetic [16–18].

In the present work, we have tracked RTFM in the Co-substituted ZnO thin films which have been deposited by spray pyrolysis. It may be noted here that for deposition of the ZnO:Co thin films, we have employed same precursors, which were used for preparation of nanocrystalline ZnO:Co powder samples. The preliminary results of their structural, optical, and magnetic properties are presented.

2 Experimental details

The $Zn_{1-x}Co_xO$ (with x = 0, 0.05 and 0.10) thin films were spray deposited on quartz and glass substrates. Zinc acetate

K. P. Bhatti · S. Chaudhary (✉)
Thin Film Laboratory, Department of Physics, Indian Institute of Technology Delhi, New Delhi 110016, India
e-mail: sujeetc@physics.iitd.ac.in

V. K. Malik
Department of Physics, University of Fribourg, Chemin du Musse 3, Fribourg 1700, Switzerland

dihydrate [$Zn(CH_3COO)_2{\cdot}2H_2O$] and cobalt acetate tetrahydrate [$Co(CH_3COO)_2{\cdot}4H_2O$] were used as precursors; and their powders in the desired molar ratio were dissolved in methanol. The molarity of the solution was maintained at 0.4 M. The substrate temperature was maintained 380 °C during the deposition of films. The flow rates of the carrier gas and the solution were maintained at 0.2 kg/cm^2 and ~20 mL/min, respectively. The film deposition was carried out for 15 min in air ambient. The phase analysis of the resulting thin films was performed by employing the glancing angle X-ray diffractometer (Philips, X'Pert PRO). Vibrating sample magnetometer (Model P525) option with PPMS from Quantum design (Model QD6000) was employed for magnetization (M) versus applied field strength (H) investigations of these thin films. A double beam spectrophotometer (Perkin-Elmer-900) was employed for studying the optical properties of these ZnO:Co films in UV–VIS range. The surface morphology of the films was studied by Atomic Force Microscope using Nanoscope (Model *IIIa*, Digital Instruments).

3 Results and discussion

Figure 1 shows the glancing angle X-ray diffractograms (XRD) of the spray deposited $Zn_{1-x}Co_xO$ thin films with x = 0.0, 0.5 and 0.10. In these diffractograms, all the observed peaks were found to correspond to wurtzite structure of ZnO. In addition, the films were found to be textured along [100]. No peaks corresponding to either Co metal or any of its oxides were observed in any of the diffractograms, which indicates that there is no additional phase present in $Zn_{1-x}Co_xO$ films, at least with in the limit of X-ray detection (0.5%).

Table 1 shows the lattice parameter 'a', full width at half maxima (FWHM, B_r) of (100) peak, the calculated crystallite size and lattice strain of different thin film samples of $Zn_{1-x}Co_xO$. The lattice parameter 'a' was calculated using (100)—the most intense peak. As seen from the Table 1, the lattice parameter 'a' for $Zn_{1-x}Co_xO$ samples is found to be smaller than that of pure ZnO. This decrease in 'a' is indicative of substitution of Co^{2+} in the ZnO lattice, since the ionic radii of Co^{2+} (0.58 Å) is smaller than that of Zn^{2+} (0.60 Å) in the tetrahedral coordination. Similar small decrease in the lattice parameter on Co addition in ZnO was reported previously also [10]. It may be mentioned here that if Co^{2+} ions were present in the octahedral environment, it would be signaled by significant increase in cell volume since octahedral Co^{2+} has an ionic radius of either 0.65 Å (low spin) and of 0.74 Å (high spin state) [19]. It is to be noted that Co^{3+} ion, though of smaller ionic radii does not readily enter the tetrahedral coordination [19].

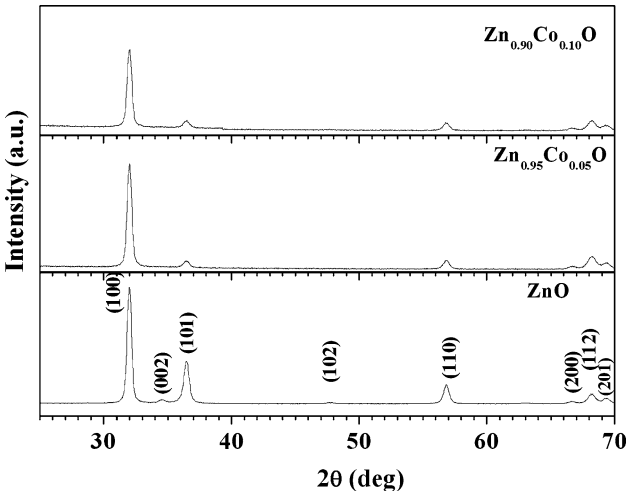

Fig. 1 Glancing angle X-ray diffraction patterns of the $Zn_{1-x}Co_xO$ thin films with x = 0.0, 0.05 and 0.10

Table 1 The lattice parameter 'a', FWHM of (100) peak, the calculated crystallite size and lattice strain of the various thin film samples of $Zn_{1-x}Co_xO$

Sample	'a' (Å)	FWHM (°)	Crystallite size (nm)	Strain
ZnO	3.235	0.336	75	3.2×10^{-3}
$Zn_{0.95}Co_{0.05}O$	3.230	0.413	54	8.6×10^{-3}
$Zn_{0.90}Co_{0.10}O$	3.228	0.438	54	13.6×10^{-3}

It is known that the peak broadening occurs due to decrease in crystallite size and also due to increase in the lattice strain. The FWHM, B_r, of the diffraction peaks, after subtracting the instrumental broadening effect, can be considered as a sum of the two contributions,

$$B_r = B_{crystallite} + B_{strain}$$

$$B_r = 0.9\lambda/(L\cos\theta) + \eta\tan\theta$$

where $B_r^2 = B_o^2 - B_i^2$, with B_o and B_i representing the FWHM of the diffraction peak for the present film sample and a standard Si, respectively. Further, λ is the wavelength of X-rays used, L is the crystallite size, and η is the lattice strain. Multiplying above equation with cos θ, we get

$$B_r\cos\theta = 0.9\,\lambda/L + \eta\sin\theta$$

The average crystallite size and strain can, therefore, be calculated by plotting the $B_r\cos\theta$ versus $\sin\theta$ for the observed XRD peaks. The slope of the plot gives the strain, whereas, the intercept yields the crystallite size. The broadening of the peak increases rapidly with the increase in θ due to both crystallite size and lattice strain, but the difference between these two contributions is distinct at smaller values of θ. It is, therefore, desirable to use diffraction peaks at smaller diffraction angles to separate the

two effects. Hence, the crystallite size and the strain were calculated using (100), (101) and (110) peaks in the X-ray diffraction patterns. These values are given in Table 1. It may be noted from Table 1, that the FWHM is seen to increase with the increase in Co concentration in the films. This could be attributed due to both the decrease in the crystallite-size from a value of 75 nm in pure ZnO to a values of ~50 nm in ZnO:Co (10%) film, and a decrease in the crystallinity of the ZnO:Co film on cobalt incorporation, which is indicated by the increase in the lattice strain. This could be associated to an increase in the number of defects. It is thus concluded that cobalt substitution definitely affects the crystalline structure of ZnO thin films, in the present case.

To study the optical properties of $Zn_{1-x}Co_xO$ thin films, the transmission spectra of the thin films with x = 0.0, 0.5 and 0.10 were recorded in a wavelength range of 200–1,200 nm, using a double-beam spectrophotometer. The transmission spectra of these films, recorded at room temperature, are shown in Fig. 2. It may be noticed that in addition to the occurrence of absorption edge in the range of 370–400 nm corresponding to the band gap of $Zn_{1-x}Co_xO$ films having different cobalt concentration, additional absorption peaks appear in the case of Co substituted ZnO films. These peaks/dips in the transmission curves are observed at 568, 616 and 660 nm. None of these absorptions correspond to the band edge of cobalt oxide. To confirm this statement, a film of cobalt oxide was spray deposited using cobalt acetate tetrahydrate solution. The XRD pattern of the film revealed that Co_3O_4 was the oxide of cobalt that is formed. An optical transmission spectrum of pure Co_3O_4 thin film was also carried out and is also shown in Fig. 2. The spectrum of Co_3O_4 has an absorption edge at ~816 nm (1.6 eV) corresponding to its band gap.

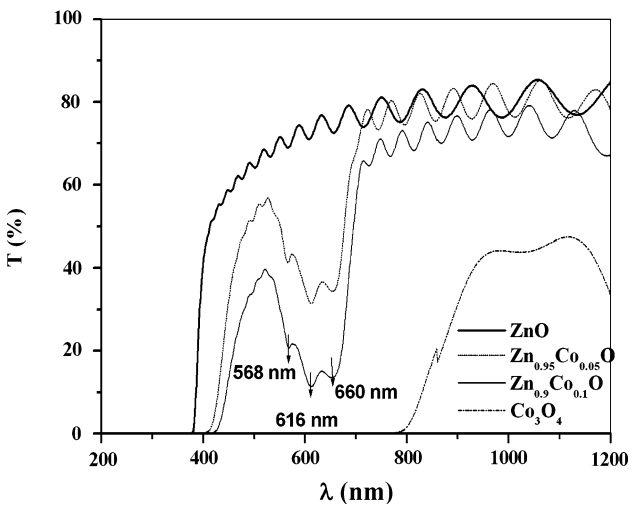

Fig. 2 The transmission spectra of $Zn_{1-x}Co_xO$ thin film samples with x = 0.0, 0.05 and 0.10, and Co_3O_4

Since no absorption at this wavelength is seen in any of the transmission spectra of $Zn_{1-x}Co_xO$ thin films, it implies that Co_3O_4 phase is not present in any of the $Zn_{1-x}Co_xO$ films. This substantiates the XRD results of these films, which do not show any peaks corresponding to Co_3O_4. The observed characteristic absorption bands (at 568, 616 and 660 nm) are due to interatomic d–d transitions among Co^{+2} ions associated with the tetrahedral crystal field splitting in ZnO lattice as explained below.

A Co^{+2} cation is in $3d^7$ configuration. According to Hund's rule and Pauli's exclusion principle, the electronic ground state configuration has L = 3 and S = 3/2. So, the ground state spectral term is ^4F and the excited state terms are ^4P, ^2G, ^2F, ^2D and ^2P [20]. However, when the Co^{2+} exists in the tetrahedral field, the ^4F term splits into $^4A_2(F)$, $^4T_2(F)$ and $^4T_1(F)$, with $^4A_2(F)$ being lowest in energy and the remaining two having higher energies. The ^4P term corresponding to the first excited state does not split, but is transformed into $^4T_1(P)$. Similarly, ^2G splits into $^2A_1(G)$, $^2E(G)$, $^2T_1(G)$ and $^2T_2(G)$. In the ground state, the atom is in $^4A_2$ state. When the electron has sufficient energy, it can be excited to higher energy states. The absorption peaks observed at 568, 616 and 660 nm (see Fig. 2) correspond to the following transitions:

$$^4A_2(F) \rightarrow {}^2A_1(G) \qquad 568\,\text{nm}$$

$$^4A_2(F) \rightarrow {}^4T_1(P) \qquad 616\,\text{nm}$$

$$^4A_2(F) \rightarrow {}^2E(G) \qquad 660\,\text{nm}$$

The observation of these transitions in the transmission spectra of our $Zn_{1-x}Co_xO$ films (Fig. 2) thus clearly reveals that the added cobalt atoms have substituted Zn^{+2} cations and are present in +2 state. This conclusion thus substantiates our inference drawn from the structural characterization about substitution of Zn^{+2} by Co^{+2} in ZnO:Co films. It may be further noted that the intensity of the absorption dips increases with increase of cobalt concentration in the $Zn_{1-x}Co_xO$ films. The area under the Co^{2+} absorption peaks increases proportionally to the Co concentration in the spray solution. This again reveals that with increase in Co concentration in $Zn_{1-x}Co_xO$ films, more and more cobalt goes into the ZnO lattice.

In addition, it may also be noted from Fig. 2 that with increase in 'x' the absorption edge shifts to lower energy side. This red shift of E_g edge with more and more Co^{+2} going into ZnO lattice can be explained by *sp-d* exchange interaction between the band electron and localized d-electron of the Co^{+2} substituting for Zn^{+2} ions. The *s-p* and *p-d* exchange interactions give rise to a negative and a positive correction to conduction and valance band edges, leading to narrowing of the band gap [21].

The surface microstructure and morphology at nanometric scale in these $Zn_{1-x}Co_xO$ thin films were studied by

atomic force microscopy (AFM). As seen from AFM images in Fig. 3, the films are uniform and densely packed. All the films understandably exhibit granular structure. It appears that the incorporation of cobalt atoms does not significantly affect the microstructure and surface morphology. The average particle size and the rms (root mean square) values of the roughness estimated from the AFM micrographs are given in Table 2. It may be noted that all the films have an rms roughness in the range of 12–18 nm and have an average particle size in the range of 80–110 nm. The crystallite sizes, as inferred from the AFM micrographs are bigger than that obtained from the XRD patterns (See Table 1). This suggests that the bigger particles seen in AFM micrographs are due to the agglomeration of small crystallites. Since the $Zn_{1-x}Co_xO$ films are deposited under same growth conditions (i.e., identical deposition temperature and on the same substrate), not much change in the microstructure is expected. Thus, Co addition in ZnO films does not cause any significant change in the surface morphology and microstructure as revealed from the nanoscopic studies.

The magnetic properties of the $Zn_{1-x}Co_xO$ thin films were studied by carrying out room temperature magnetization versus field (M–H) measurements. The DC-magnetic field was applied parallel to the film plane. The M–H measurements of the quartz substrate and pure ZnO thin film were also carried out. The M–H plot of the quartz substrate (as shown in Fig. 4), is found to be linear with a negative slope, indicating a pure diamagnetic behavior. For the $Zn_{0.95}Co_{0.05}O$ and $Zn_{0.90}Co_{0.10}O$ samples, a distinct non-linearity was observed in the as recorded M–H data (see Fig. 5). It is observed that the non-linearity increases with the increase in cobalt concentration in the films. It is clear from the Fig. 5 that the observed M–H behavior of the samples is a collective result of a large diamagnetic contribution, together with a small ferromagnetic component. As mentioned above, the diamagnetic behavior is due to the substrate (together with the sample holder) and the observed ferromagnetic contribution results from the $Zn_{1-x}Co_xO$ films. The ferromagnetic fraction is extracted from the raw data by subtracting the diamagnetic contribution calculated from the slope of the high field linear M–H region. The extracted M–H loop of this corresponding to the FM phase present in the film is shown in Fig. 6. It may be mentioned here that in all the measurements, the film-samples of approximately same area (3×5 mm^2) were employed so as to have approximately the same mass of the film.

Table 2 RMS roughness and the average particle size of $Zn_{1-x}Co_xO$ thin films as estimated from the AFM micrographs

Sample	RMS roughness (nm)	Average particle size (nm)
ZnO	17	84
$Zn_{0.95}Co_{0.05}O$	12	84
$Zn_{0.90}Co_{0.10}O$	18	83

From the foregoing, it turns out that for the same film mass, the saturation moment of the $Zn_{1-x}Co_xO$ films increased only slightly with increase in Co concentration. It may be noted that the appearance of saturated hystersis loop (see inset of Fig. 6) by a small applied field (300 mT) precludes the presence of superparamgnetic clusters. In a separate work, we have analyzed in detail high field M–H data (up to 9 T) in the temperature range of 10–300 K of these $Zn_{1-x}Co_xO$ thin films [22]. Recall that in these thin films, either little (undetected) or no cobalt oxide is formed (as concluded from the XRD and optical results). Absence of cobalt oxide is expected since the films were deposited for a small duration of $\sim$15 min which has understandably enhanced the solubility of Co in ZnO due to the well known non equilibrium nature of the thin film growth process. Since the films are deposited at fairly high temperature ($\sim$380 °C) in ambient condition, presence of clusters of cobalt is altogether ruled out (consistent with our XRD results). Thus, the observed magnetic behavior cannot be ascribed to the presence of cobalt-clusters. Further, the oxides of cobalt (Co_3O_4 and CoO) and the known compounds of ZnO and Co (e.g., $ZnCo_2O_4$) are paramagnetic at room temperature and hence, cannot result in the observed RTFM. Based on the results of our thin film samples, it is concluded that the observed RTFM cannot be

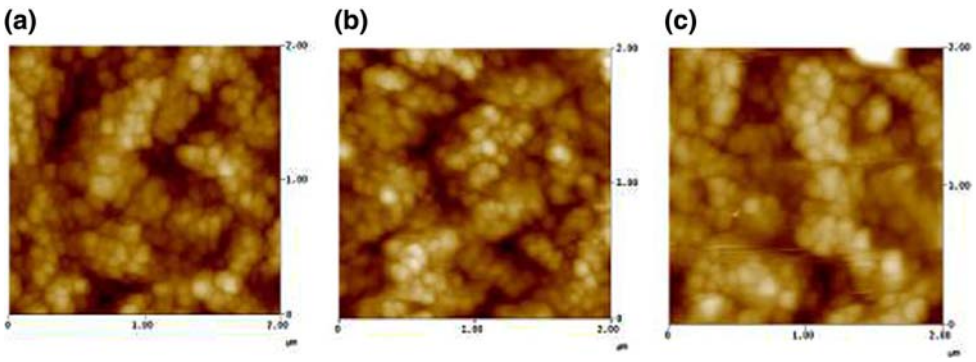

Fig. 3 The 2D AFM pictures (**a**) ZnO, (**b**) $Zn_{0.95}Co_{0.05}O$ and (**c**) $Zn_{0.9}Co_{0.1}O$

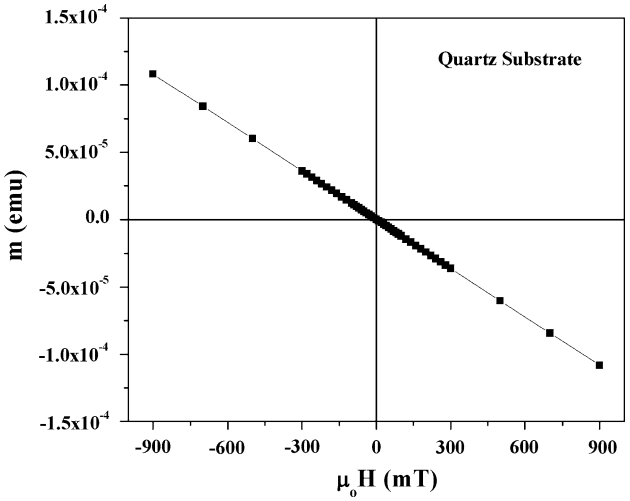

Fig. 4 The M–H plot recorded at 300 K of quartz substrate

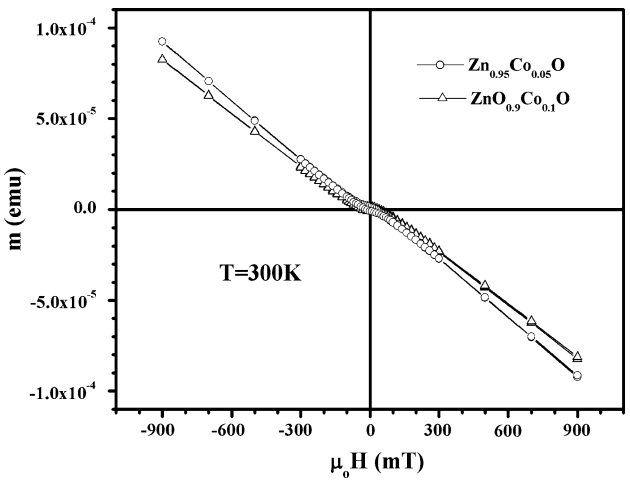

Fig. 5 As recorded M–H plots $Zn_{0.95}Co_{0.05}O$ and $Zn_{0.9}Co_{0.1}O$ thin films (T = 300 K)

ascribed to Co clusters and must be an intrinsic effect of cobalt incorporation into ZnO lattice.

Since these films possess high resistivity ($\sim 10^7$ Ωm), the observed RTFM could be associated with the formation of bound magnetic polarons [23], similar to the case of our nanocrystalline $Zn_{1-x}Co_xO$ powder samples [3–5]. Coey et al. [24] have alternatively ascribed origin of FM to defect related magnetic ordering. It may be recalled that, in the present case, the AFM micrographs of these films suggest that there was no change in the microstructure due to Co incorporation, although, an increase in the strain and decrease in the crystallinity was evidenced. Thus, alternatively, the observed increase in RTFM with increase in cobalt concentration in the present films could be defect mediated. Due to lack of any conclusive/definite evidence in favor of this possibility, a firm correlation of RTFM with either defect related magnetic ordering or bound magnetic polarons cannot be established yet.

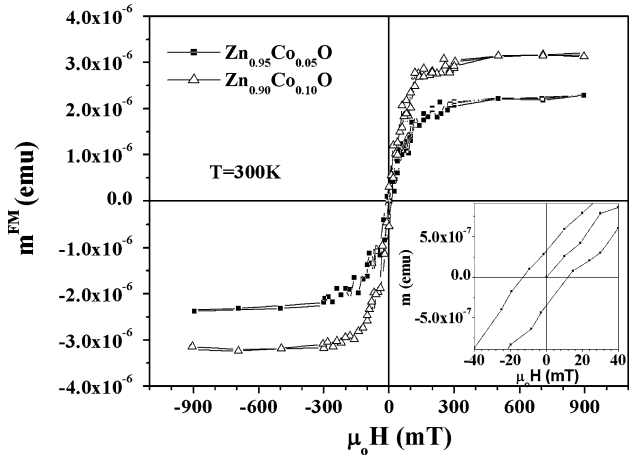

Fig. 6 The magnetization versus field behavior of the ferromagnetic phase extracted from the raw data for the $Zn_{0.95}Co_{0.05}O$ and $Zn_{0.9}Co_{0.1}O$ thin films. The inset shows the enlarged view if the hystersis loop of $Zn_{0.95}Co_{0.05}O$ thin film

4 Conclusions

Thin films of $Zn_{1-x}Co_xO$ (with $x \leq 0.10$) were deposited by spray pyrolysis technique on quartz/glass substrates. These films exhibit room temperature ferromagnetic ordering. The XRD results indicate that the films have wurtzite structure and are preferentially [100] textured. The small change in the lattice parameter 'a' with x, is consistent with the incorporation of Co^{2+} in the ZnO lattice. No X-ray evidence of metallic cobalt or any of oxides of cobalt is found in these thin films. The $Zn_{1-x}Co_xO$ films having different Co concentration have almost similar surface morphology and microstructure. The optical transmission spectrum of the film evidenced (i) the presence of d–d band transitions, (ii) shift of absorption edge to lower energy values with increase in cobalt concentration, and (iii) the systematic variation of the intensity of absorptions of d–d band with the increase in cobalt concentration. These observations conclusively prove that in these films Co exits in +2 states at tetrahedral sites and substitutes Zn^{2+}. In view of insulating nature of these $Zn_{1-x}Co_xO$ thin films, the observed magnetic ordering at room temperature can possibly be attributed due to either bound magnetic polaron model or defect mediated spin split model.

Acknowledgments One of the authors (KPB) acknowledges CSIR, India for the research fellowship. Authors also acknowledge DIT/MHRD, Govt. of India for financial grant, and the technical support provided by Mr. Nagendra Chaudhary and Mr. Girija Bhushan Dash of the laboratory.

References

1. T. Dietl, H. Ohno, F. Matsukur, J. Cibert, D. Ferrad, Science **287**, 1019 (2000)
2. K. Sato, H. Katayama-Yoshida, Jpn. J. Appl. Phys. Part 2 **39**, L555 (2000)
3. K.P. Bhatti, S. Kundu, S. Chaudhary, S.C. Kashyap, D.K. Pandya, J. Phys. D: Appl. Phys. **39**, 4909 (2006)
4. K.P. Bhatti, S. Chaudhary, D.K. Pandya, S.C. Kashyap, J. Appl. Phys. **101**, 033902 (2007)
5. K.P. Bhatti, S. Chaudhary, D.K. Pandya, S.C. Kashyap, J. Appl. Phys. **101**, 103919 (2007)
6. C. Song, K.W. Geng, F. Zheng, X.B. Wang, Y.X. Shen, F. Pan, Y.N. Xie, T. Liu, H.T. Zhou, Z. Fan, Phys. Rev. B **73**, 024405 (2006)
7. S. Ramachandran, A. Tiwari, J. Narayan, Appl. Phys. Lett. **84**, 5255 (2004)
8. D.A. Schwartz, D.R. Gamelin, Adv. Mater. **16**, 2115 (2004)
9. P. Sati, R. Hyan, R. Kuzian, S. Regnier, S. Schafer, A. Stepanov, C. Morhain, C. Deprais, M. Laugt, M. Goiran, Z. Golacki, Phys. Rev. Lett. **96**, 017203 (2006)
10. L. Yan, C.K. Ong, X.S. Rao, J. Appl. Phys. **96**, 508 (2004)
11. Z.W. Jin, T. Fukumura, K. Hasegawa, Y.Z. Yoo, K. Ando, T. Sekigucji, P. Ahmet, T. Chikyow, T. Hasegawa, H. Koinuma, M. Kawasaki, J. Cryst. Growth **237–239**, 548 (2002)
12. J. Cui, Q. Zheng, U.J. Gibson, J. Appl. Phys. **99**, 08M113 (2006)
13. J.H. Park, M.G. Kim, H.M. Jang, S. Ryu, Y.M. Kim, Appl. Phys. Lett. **84**, 1338 (2004)
14. J.H. Kim, H. Kim, D. Kim, Y.E. Ihm, W.K. Choo, J. Appl. Phys. **92**, 6066 (2002)
15. M. Tay, Y. Wu, G.C. Han, T.C. Chong, Y.K. Zheng, S.J. Wang, Y. Chen, X. Pan, J. Appl. Phys. **100**, 63910 (2006)
16. T. Shi, S. Zhu, Z. Sun, S. Wei, W. Liu, Appl. Phys. Lett. **90**, 102108 (2007)
17. Y.B. Zhang, T. Srirharan, S. Li, Phys. Rev. B **73**, 172404 (2006)
18. P.S. Yin, M.X. Xu, L. Yang, J.F. Liu, H. Rösner, H. Hahn, H. Gleiter, D. Schild, S. Doyle, T. Liu, T.D. Hu, E. Takayama-Muromachi, J.Z. Jiang, Phys. Rev. B **73**, 224408 (2006)
19. R.D. Shannon, C.T. Prewitt, Acta Crystallogr. B: Struct. Crystallogr. Cryst. Chem. **25**, 925 (1969)
20. J.D. Lee, in *Concise Inorganic Chemistry*, 5th edn. (ELBS with Chapman and Hall, London, 1996) p. 947
21. J.K. Furdyna, J. Appl. Phys. **64**, R29 (1988)
22. K.P. Bhatti, V.K. Malik, S. Chaudhary, D.K. Pandya, S.C. Kashyap, to be published
23. A. Kaminski, S.D. Sarma, Phys. Rev. Lett. **88**, 247202 (2002)
24. J.M.D. Coey, M. Venkatesan, C.B. Fitzgerald, Nat. Mat. **4**, 173 (2005)